Eur. Phys. J. D **28**, 39–48 (2004)
DOI: 10.1140/epjd/e2003-00296-0

THE EUROPEAN PHYSICAL JOURNAL D

Subharmonic excitation of the eigenmodes of charged particles in a Penning trap

G. Tommaseo, P. Paasche, C. Angelescu, and G. Werth[a]

Johannes Gutenberg Universität, Institut für Physik, 55099 Mainz, Germany

Received 24 July 2003 / Received in final form 22 September 2003
Published online 2nd December 2003 –

Abstract. When parametrically excited, a harmonic system reveals a nonlinear dynamical behaviour which is common to non-deterministic phenomena. The ion motion in a Penning trap — which can be regarded as a system of harmonic oscillators — offers the possibility to study anharmonic characteristics when perturbed by an external periodical driving force. In our experiment we excited an electron cloud stored in a Penning trap by applying an additional quadrupole r.f. field to the endcaps. We observed phenomena such as individual and center-of-mass oscillations of an electron cloud and fractional frequencies, so-called subharmonics, to the axial oscillation. The latter show a characteristic threshold behaviour. This phenomenon can be explained with the existence of a damping mechanism affecting the electron cloud; a minimum value of the excitation amplitude is required to overcome the damping. We could theoretically explain the observed phenomenon by numerically calculating the solutions of the damped differential Mathieu equation. This numerical analysis accounts for the fact that for a weak damping of the harmonic system we observed an even-odd-staggering of the the different orders of the subharmonics in the axial excitation spectrum.

PACS. 52.27.Jt Nonneutral plasmas – 82.80.Qx Ion cyclotron resonance mass spectrometry

1 Introduction

Penning traps confine charged particles by a combination of a static electric quadrupole potential Φ and a superimposed magnetic field $\boldsymbol{B}$ in axial direction. The scalar quadrupole potential is described by

$$\Phi = \frac{U_0}{r_0^2 + 2z_0^2}\Big(r^2 - 2\left(z^2 - z_0^2\right)\Big) \tag{1}$$

with $r^2 = x^2 + y^2$ and the magnetic field follows from a vector potential

$$\boldsymbol{A} = \frac{1}{2}\boldsymbol{B} \times \boldsymbol{r} \equiv \frac{1}{2}B(-y\hat{e}_x + x\hat{e}_y) \tag{2}$$

when $\boldsymbol{B} = B\hat{e}_z$ is along the z-symmetry axis. U_0 is the voltage applied to the hyperbolic shaped ring and endcap electrodes (see Fig. 1) of characteristic dimension $r_0^2 + 2z_0^2 = d^2$, where r_0^2 is the radius of the ring electrode and $2z_0$ is the distance between the endcaps. The form of the potential in (1) suggests that the trapping voltage U_0 is applied to the ring electrode and to the endcaps are grounded: $\Phi(r = r_0, z = 0) = U_0$ and $\Phi(x = 0, y = 0, z = z_0) = 0$. The Penning trap serves for a number of different purposes: high precision measurements of magnetic moments [1–3], accurate mass comparison [3–6], or investigation of strongly coupled plasmas [7,8]. In these experiments the trap acts as a container which keeps the charged particles in a localized volume and makes them available for laser spectroscopic or mass spectrometric experiments in a well controlled environment.

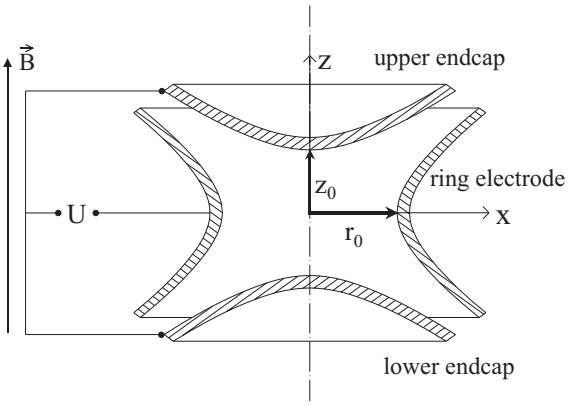

Fig. 1. Sketch of the hyperbolic Penning trap.

The dynamics of trapped particles has also been subject to experimental [9–11] and theoretical investigations [12]. The stored ion or electron behaves essentially as an oscillator which in the absence of deviations from the ideal quadrupole potential is purely harmonic. Higher

[a] e-mail: werth@mail.uni-mainz.de

order terms in the potential arising from trap imperfections or space charge effects lead to anharmonicities in the particle's motion. Because of the conceptual simplicity of the device it can be used to investigate the dynamics of motion in some detail. In previous experiments in our laboratory [13] we have shown that the existence of higher order parts in the trapping potential lead to instabilities in the ion motion when the electric and magnetic fields are chosen in such a way that the following relation is fulfilled:

$$\ell_+\omega_+ + \ell_-\omega_- + \ell_z\omega_z = 0 \tag{3}$$

where (ℓ_+, ℓ_-, ℓ_z) is a triple of integer numbers and the frequencies ω_j, $j \in \{+, -, z\}$ result from the solutions of the Euler-Lagrange equations of charged particle moving in a static electric quadrupole field and a homogeneous magnetic field:

$$\frac{d}{dt}\frac{\partial \mathcal{L}}{\partial \dot{q}_i} - \frac{\partial \mathcal{L}}{\partial q_i} = 0 \tag{4}$$

where $q_i \in \{x, y, z\}$ and $\dot{q}_i \in \{\dot{x}, \dot{y}, \dot{z}\}$ are respectively the canonical space and momentum coordinates and

$$\mathcal{L} = \frac{1}{2m}(\boldsymbol{p} + q\boldsymbol{A})^2 + q\Phi \tag{5}$$

is the Lagrangian. The solutions of the set of equations in (4) give three harmonic oscillations, called the axial, the magnetron and the perturbed cyclotron motion with respective frequencies:

$$\omega_z = \sqrt{-\frac{2qU_0}{mr_0^2}} \tag{6}$$

$$\omega_- = \frac{\omega_c}{2} - \sqrt{\frac{\omega_c^2}{4} - \frac{\omega_z^2}{2}} \tag{7}$$

$$\omega_+ = \frac{\omega_c}{2} + \sqrt{\frac{\omega_c^2}{4} - \frac{\omega_z^2}{2}} \tag{8}$$

$\omega_c = eB/m$ is the particles' free cyclotron frequency. In the absence of anharmonic perturbations a massive charged particle confined in an ideal hyperbolic shaped Penning trap can be regarded as a multiperiodic system. By transforming this harmonic motion in a rotating frame S_Ω spinning around the symmetry z-axis at the angular velocity $\Omega = -\omega_c/2$ with respect to the laboratory frame at rest, the hyperbolic shaped trap is equivalent to a three-dimensional oscillator moving in the radial plane and in the axial direction with the frequencies $(\omega_+ - \omega_-)/2$ and ω_z, respectively [14,15]. The static anharmonic perturbations considered in the experiment of reference [13] have its origin in the limitation of the technical realization of the Penning trap used in the laboratory.

In this paper we present measurements on electrons in a Penning trap which were additionally subject to a time dependent perturbation. We show that the excitation of their axial motion by an additional weak r.f. field leads to the appearance of fractional frequencies in the motional spectrum. These subharmonics to the axial motion are a fundamental characterization of nonlinear dynamical systems when parametrically excited by an external periodical driving force. Similar observation were made on stored N_2^+ [16], N^+ [17] and H_2^+ [18] molecules in a Paul trap, where the confinement of charged particles is obtained by an a.c. field applied additionally to a static electric field to the same electrode configuration as in case of the Penning trap.

1.1 Parametric excitation

It is a well-known fact that the excitation of a harmonic system with an eigenfrequency ω at a frequency 2ω leads to an oscillation at the frequency ω. We call this phenomenon a parametric excitation [19–21] because the perturbation acting on the harmonic system is a characteristic quantity of the system itself. Moreover the system is excited at fractional frequencies $2\omega/n$, $n \in \mathbb{N}\setminus\{0\}$, so called subharmonics. In the case of a parametric excitation the increment of energy which is transfered by the external excitation to the oscillating system is proportional to the stored energy in the system itself and decreases with higher order n of the parametric resonance. Moreover the friction — which is present in every real harmonic system — also depends linearly on the velocity of the oscillating system. So the ratio between the investment of energy due to the parametric excitation and the energy dissipation due to frictional losses does not depend on the amplitude. As a consequence the increment of the energy caused by the external periodical perturbation has to exceed the amount of energy dissipated during the same time, in order to see the parametric resonances.

In the 30s Mandelstam and coworkers [22,23] started a fundamental investigation on the theory of subharmonics, which was essentially based on Poincarés tract on celestial mechanics [24]. They built, as they called it, a *parametric generator* consisting of an electric tank circuit and a variable parameter being a capacitance or an inductance. A more general approach elaborating a mathematical method was taken by Ljapunow. His stability theory could also be extended to non-conservative systems, i.e. the theory describes linear and nonlinear differential equations with periodic coefficients [25]. If the coefficient is a time dependent *cosinus* function, we obtain as a special case the Mathieu differential equation [26] for the amplitude u of the system:

$$\frac{d^2u}{d\tau^2} + (a - 2q\cos 2\tau)u = 0 \tag{9}$$

a and q are the so-called stability parameters and $\tau = \Omega t/2$ is the time normalized to the frequency Ω of the parameter. By applying the Floquet theorem [27] a set of stable and unstable solutions can be obtained which can be graphically represented in a *Strutt diagram* [28] (Fig. 2). This diagram has stable and unstable regions in the "parameter space" (a, q) corresponding to the undashed and dashed areas, respectively.

The damped Mathieu differential equation, which has additionally a constant linear damping term, can be treated mathematically in the same way leading to the

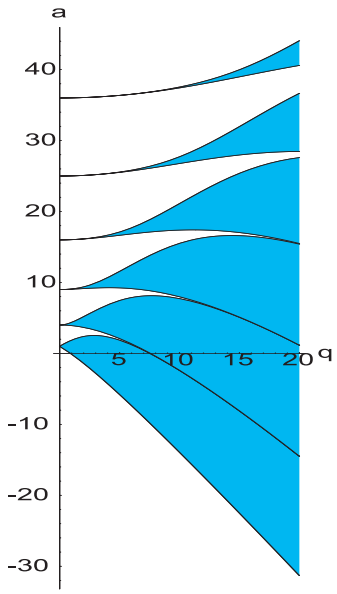

Fig. 2. Strutt diagram of the Mathieu differential equation. The shaded areas belongs to infinite temporal solutions and are called unstable.

calculation of Hill determinants [29] in order to get the solutions of the set of equations. First quantitative theoretical calculations analysing the influence of the damping term on the unstable regions of the Strutt diagram were performed by Kotowski [30]. The most important result is that the damping term reduces the unstable areas in such a way that the instability occurs at a certain threshold value of the parameter q, depending on the damping constant of the harmonic system and on the excitation amplitude of the external periodical driving force.

2 Experiment

For our investigation we use electrons since they are easy to produce and the detection features are identical to the one we apply for a magnetic field calibration within the context of double resonance experiments [11]. Our results, however, are independent of the nature of the trapped particles and apply to heavy ions as well. Our trap has a ring radius of $r_0 = 12.7$ mm and an endcap distance of $2z_0 = 18$ mm thus fulfilling the standard design in which $r_0 = \sqrt{2}z_0$ [31]. This hyperbolic shaped trap is placed in an ultra-high vacuum vessel at a base pressure of 2×10^{-9} mbar. The magnetic field is provided by a superconducting solenoid and has a strength of 2.87 T. Typical trapping voltages U_0 are about 15 V. The trap is loaded by electrons coming from a tungsten wire placed 10 cm outside the lower endcap electrode (see Fig. 3). They are injected through a 1 mm hole into the trap by an electric pulse of typically 10 ms duration. Detection of the trapped electrons is through their axial motion: we connect the two endcaps by an inductance L which forms a tank circuit together with trap electrodes acting as a capacitance C (Fig. 4). The circuit is weakly excited at its resonance

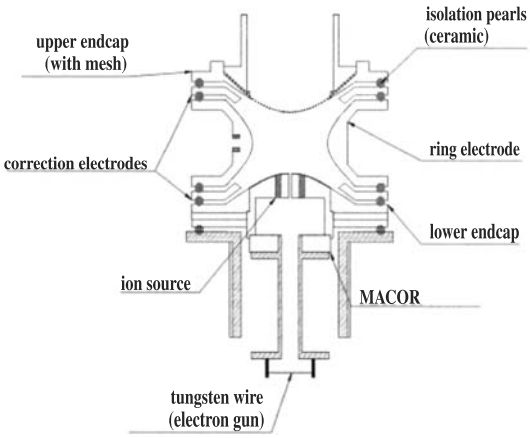

Fig. 3. Penning trap as use in our experiment. The magnetic field is directed along the vertical axis.

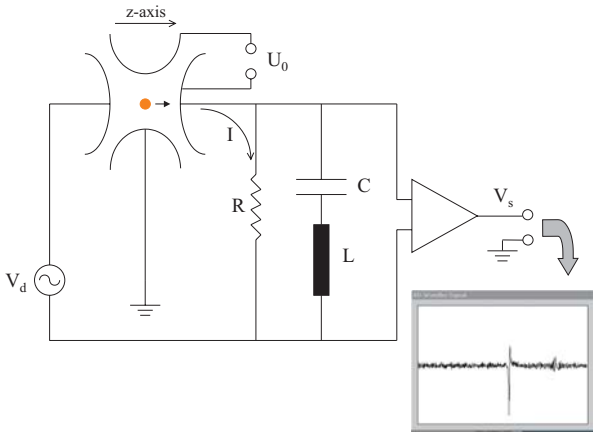

Fig. 4. Sketch of the external tank circuit connected to the endcaps of the trap. The current I created by the induced image charges flows through a resistance R which is part of the tank circuit. V_d denominates the external periodical driving force which parametrically excites the electrons. The picture in the frame on the right side shows a detection signal of the trapped electrons. The rectified damping signal of the LC circuit is proportional to the number of stored electrons.

frequency $\omega_{LC}/2\pi = 13$ MHz. When the trapping voltage U_0 is varied the axial electron oscillation frequency ω_z changes according to equation (6). At a certain voltage (about 5 V) ω_z is equal to ω_{LC}. Then the electrons absorb energy and the circuit is damped. By measuring the voltage drop across the circuit we observe a decrease in case of resonance. After rectification and demodulation we obtain a signal whose amplitude is proportional to the number of trapped electrons (see Fig. 4). It is digitized and further handled by a personal computer. After detecting the electrons the voltage ramp continues until the trapping potential changes sign and the electrons leave the trap. This assures that every loading-detection cycle starts with identical initial conditions and no "memory effect" of electrons left in the trap occurs.

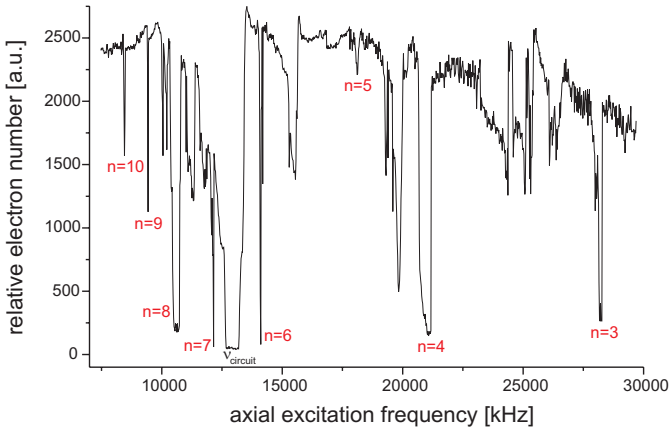

Fig. 5. Axial excitation spectrum showing subharmonics at $\omega = 2\omega_z/n$, n ranging from 2 to 10 taken at a trapping voltage of $U_0 = 40$ V.

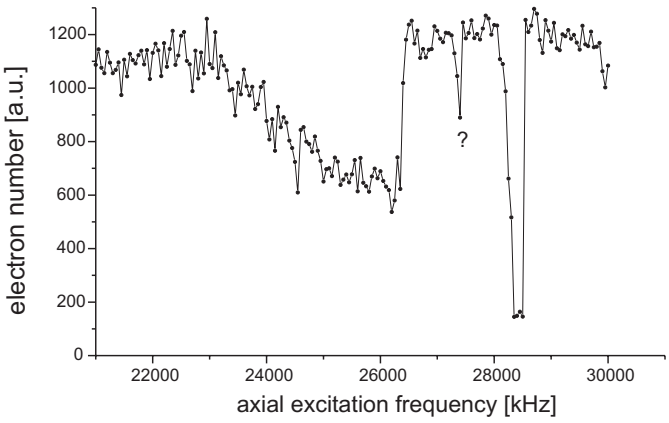

Fig. 6. Excitation at $\omega - 2\omega_z$ individual (lower frequency side) and center-of-mass (higher frequency side) resonances.

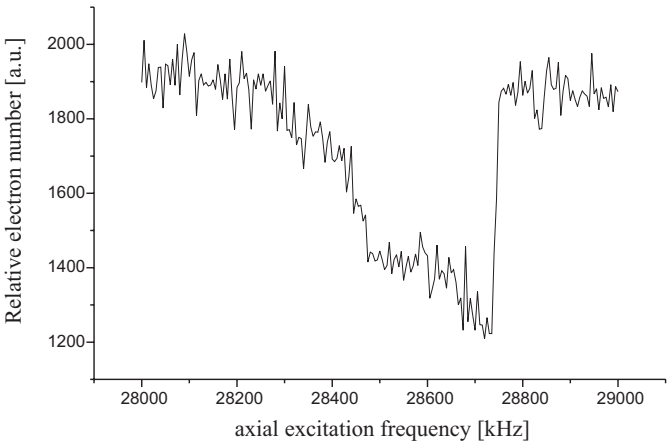

Fig. 7. The center-of-mass resonance taken with high resolution.

2.1 Fractional frequencies

If a parameter of a harmonic system is excited at a frequency which is twice as high as the eigenfrequency of the system, i.e. 2ω, then the system itself starts oscillating at a frequency ω. Additionally we observe resonances at the fractional frequencies $2\omega/n$. These subharmonics form the fundamental characteristic of nonlinear systems [20,32].

We excite the axial motion of the trapped electrons by an additional r.f. field (<10 mV) applied to the filament of the ion source (see Fig. 3) which we used as antenna for the radiofrequency. We assume that due to the given geometry of the trap electrodes we induce a superposition of a dipole and a quadrupole excitation. When the frequency of this field is varied and the electron oscillation is excited the electrons gain energy and some of them leave the trap. This resonant excitation is monitored by a decrease in the detection signal. Figure 5 shows an example of such a measurement where the minima in the detected electron number occur at frequencies $2\omega_z/n$, the integer number $n \in \mathbb{N}$ ranging from 3 to 10. In addition we observe resonances at different frequencies, produced by linear combination of ω_-, ω_+, ω_z, which are of no interest here. All subharmonics to the $2\omega_z$ resonance reveal a characteristic substructure which becomes evident when we scan across the resonance with high resolution. As an example we show in Figure 6 the $(n = 1)$-resonance which is most easily excited. We see a broad asymmetric resonance ($\Delta\nu \approx 3$ MHz) and a one order of magnitude smaller resonance ($\Delta\nu \approx 200$ kHz) on the higher frequency side (Fig. 6). The asymmetry of this narrow resonance is similar to the broad one (see Fig. 7 taken with higher resolution) and is a characteristic of a parametrically driven anharmonic oscillator [19]. It may give informations about higher order terms to the harmonic storage potential. This is briefly discussed in the appendix.

We can regard these two resonances as two different modes of motion of the electron cloud. The broad resonance is the excitation of the individual electrons' oscillations while at the narrow resonance the centre-of-mass of the electron cloud is excited. This becomes evident from the number dependence of the resonance frequencies: while the broad resonance shifts to lower frequencies with increasing electron number as expected from space charge, the frequency position of the narrow resonance remains constant since the centre-of-mass does not experience any space charge effect.

This "synchronous oscillation" of a cloud of charged particles was first observed by Rettinghaus [33] in 1965 on stored N_2^+ molecules in a Paul trap[1]. First indications of the same phenomenon on stored electrons in Penning traps are attributed to Wineland and Dehmelt [34]. More detailed investigations were performed by Paasche et al. [13].

The appearance of the fractional frequencies can be explained when we consider the axial motion of the electrons under the influence of the r.f. driving field. Neglecting for the moment damping terms of the harmonic system and nonlinear terms in the storage potential the equation of motion in the axial direction writes

$$\ddot{z} + \omega_z^2\, z = V_0\,(\cos\omega t)\, z \qquad (10)$$

where V_0 and ω denote the amplitude and the frequency of the excitation field, respectively. Using the transformation

[1] This information is reported in reference [16].

$\tau = \omega t/2$ equation (10) can be rewritten yielding

$$\frac{d^2z}{d\tau^2} + (a - 2q\cos 2\tau)z = 0. \tag{11}$$

The dimensionless parameters a and q are given by

$$a = \left(\frac{2\omega_z}{\omega}\right)^2 \tag{12}$$

and

$$q = \frac{2F}{\omega^2} \tag{13}$$

with $F = eV_0/mr_0^2$.

Equation (11) is a differential equation of the Mathieu-type. From the theory of Mathieu equations [27] it is known that the solutions fall into two categories depending on the values of the pair of parameters (a, q): solutions where the amplitude remains finite in time are called stable, those in which the amplitude increases to infinity with time are called unstable. For vanishing values of the parameter q the instability tongues start at $a = n^2$, $n \in \mathbb{N}$ (see Fig. 2). In our case the amplitude of the exciting field V_0 which determines the value of q is very small (<1 V) and we can reasonably assume $q \approx 0$. Then it follows immediately that the instabilities occur at the frequencies $\omega_n = 2\omega_z/n$ as experimentally observed.

The inclusion of a linear damping term $-\delta\dot{z}$ in equation (11) shifts on the one hand the starting point of the instability tongues to larger a and q values and on the other hand it reduces the instability regions. Furthermore a critical threshold amplitude is required to overcome the effect of damping and therefore to make the subharmonics visible. We can experimentally determine the critical amplitude for the different subharmonics by varying the excitation amplitude of the r.f. field and looking at the value when the resonance vanishes. Figure 8 shows such a measurement where in a semilogarithmic scale the excitation amplitude is plotted versus the width of the resonance. The intersection point of the curve with the abscissa marks the threshold value. This characteristic threshold behaviour implying a critical amplitude V_c for the different fractional resonances has been derived by Bogoljubow [32] for small q values with the asymptotic method:

$$V_{\text{crit}}^{(n)}(\delta) = \alpha_n(\delta)\delta^{1/n}. \tag{14}$$

For very low damping constant the coefficient $\alpha_n(\delta)$ has a neglegible dependence on δ [35]. When we plot the logarithm of the critical threshold amplitude versus the reciprocal value of the order of the subharmonics we expect from (14) a linear dependence with δ as slope. We find, however, that different dependencies appear for the odd and for the even values of n as seen from Figure 9. It should be noted that the experimentally determined resonances for $n = 1$ and $n = 2$ have a smaller threshold value than theoretically calculated. Since these two fractional frequencies are also excited directly through the tank circuit, the threshold value of the parametric excitation is strongly affected by this direct excitation. Therefore the threshold value is reduced.

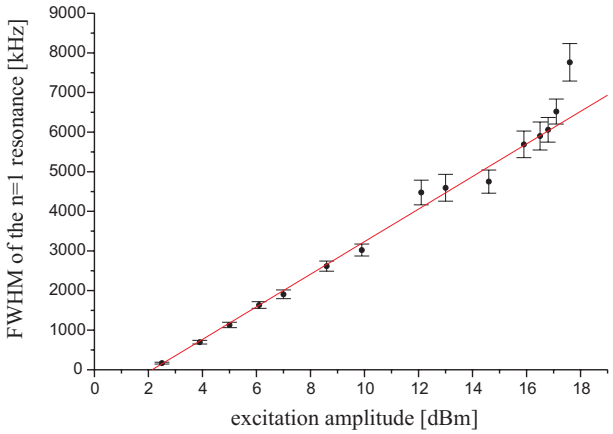

Fig. 8. Graphical plot of the width of the $2\omega_z$ resonance versus the excitation amplitude of the external driving force. The intersection point of the curve with the abscissa defines the threshold value.

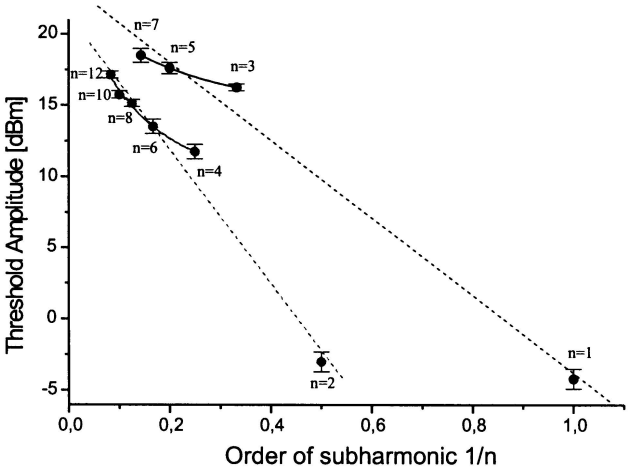

Fig. 9. Observed relative threshold amplitudes for subharmonic excitation at $\omega = 2\omega_z/n$. The dashed lines represent a linear dependence.

The same phenomenon was observed on stored N_2^+ [35] and H_2^+ [18] molecules in a hyperbolic shaped Paul trap under UHV conditions. No satisfactory explanation for this behaviour was given. Collings and Douglas made similar experiments on heavier molecular ions in a linear Paul trap at higher background pressures [36]. They observed the predicted linear dependence for all values of n without an indication of an even-odd staggering.

2.2 Damping mechanism

The damping of the electron oscillation can arise from two different effects: collisions with background gas molecules and energy dissipation when the trapped electrons are brought into resonance with the detection tank circuit as shown in Figure 4. In this case the harmonic motion of the electrons in the axial direction induces image charges in both endcaps which result in an induced current. This current flows through a resistance, which is part of the

tank circuit connected to the trap, creating thus a voltage which adds to the trapping voltage. This voltage causes a time varying axial electric field at the center of the trap which implies an axial force. The latter counteracts the electrons' motion and therefore dampens it.

To estimate the size of the damping constant δ from collisions we assume a collision rate $R = n\sigma v$ with a cross-section $\sigma \approx 10^{-16}$ cm^2 and a background gas density n of 3×10^{10} cm^{-3} at a pressure of 10^{-7} mbar which is a typical value for our experimental conditions. The relative velocity v is about 1×10^8 cm/s. This corresponds to a mean electron energy of 1.5 eV, a reasonable estimate in the 15 V potential depth as applied in our experiment. The damping constant caused by collisions $\delta_{\text{coll}} = R/\omega_z$ then amounts to about 5×10^{-6}.

Damping from the detection circuit can be estimated from the shift in the axial oscillation frequency caused by the induced image charges. The axial resonance frequency ω_z of our oscillating system in case of damping is shifted to

$$\omega_z' = \omega_z \sqrt{1 - \frac{\delta^2}{2}}. \tag{15}$$

It follows then

$$\delta^2 = \frac{2(\omega_z^2 - \omega_z'^2)}{\omega_z^2} \approx \frac{4(\omega_z - \omega_z')}{\omega_z} = \frac{4\Delta\omega_z}{\omega_z}.$$

The fractional frequency shift $\Delta\omega_z/\omega_z$ has been derived from the model of a homogeneously charged trapped particle cloud as [37,38]

$$\frac{\Delta\omega_z}{\omega_z} = \frac{Ned^2}{2a^3U_0} \tag{16}$$

where Ne is the number of charges, d the distance between the endcaps of the trap and a the radius of the particles' cloud. For $N = 10^6$, $d = 2z_0 = 18$ mm and $a \approx 1$ mm, determined by the size of the electrons' entrance hole in the endcap electrode, we obtain for our trapping voltage $U_0 = 15$ V as a fractional frequency shift $\Delta\omega_z/\omega_z = 3.6 \times 10^{-9}$. It follows for the damping constant $\delta_{\text{image}} = 1.2 \times 10^{-4}$. An alternative way to determine the damping resulting from the image charges is to look directly at the axial force F_z which is produced at the center of the trap by the induced electric field [12]:

$$F_z = -\frac{e\kappa I R_{\text{diss}}}{2z_0} \tag{17}$$

e is the elementary charge, κ is a geometrical factor of the order of one considering the curvature of the electrodes, I is the induced current which flows through the resistance R_{diss} and $2z_0$ is the distance between the two electrodes. Since the current I is proportional to the velocity $\dot{z}$ of the electron approaching the electrode, equation (17) describes a dissipative force,

$$F = -m\delta_z\dot{z} \tag{18}$$

δ_z being the damping constant of the axial motion given by [39]:

$$\delta_z = \left(\frac{e\kappa}{2z_0}\right)^2 \frac{R_{\text{diss}}}{m}. \tag{19}$$

The resistance can be determined from the knowledge of the inductance L, which cancels the trap capacitance together with the quality factor Q of the tuned tank circuit:

$$R_{\text{diss}} = Q\omega_z L. \tag{20}$$

Taking for $L = 1$ nH and for $\kappa = 0.8$, we obtain for an axial excitation frequency of $\omega_z = 2\pi \times 13$ MHz for the axial damping constant the value $\delta_z \approx 3 \times 10^{-4}$, in agreement with the estimate given above.

From these numbers it can be clearly seen that the assumption $\delta \ll 1$ is reasonable. Moreover we see that for trapped electrons the main damping mechanism comes from induced image charges.

3 Theoretical simulations

To first order we consider an additional linear damping term leading to the following damped Mathieu equation

$$\frac{d^2z}{d\tau^2} + \delta\dot{z} + (a - 2q\cos 2\tau)z = 0. \tag{21}$$

With the substitution $z(\tau) = e^{-\frac{\delta}{2}\tau}u(\tau)$ we get back the standard form of the Mathieu equation

$$\frac{d^2u}{d\tau^2} + (\tilde{a} - 2q\cos 2\tau)u = 0 \tag{22}$$

with the modified value $\tilde{a} \equiv a - \delta^2/4$.

As was demonstrated by Bogoljubow and Mitropolski [32] and Hagedorn [40] further nonlinear terms κz^3 and quadratic damping terms $\lambda\dot{z}^2\text{sgn}(z)$ to first order do not contribute to a reduction of the instability regions shown in Figure 2. We obtain a solution of equation (22) in the form

$$u = e^{\mu\tau}p(\tau) \tag{23}$$

where $p(\tau)$ is a periodic function and μ is the Floquet exponent [27] depending on the parameters $\tilde{a}$ and q. This exponent is supposed to be complex when we consider points (a, q) which lie in the unstable regions of the Strutt diagram. Therefore we make the following ansatz for μ:

$$\mu = \gamma + i\,n, \quad n \in \mathbb{N}. \tag{24}$$

Using the algebraic software Mathematica[2] we obtain the following solution for the damped Mathieu equation, assuming $z(0) = z'(0) = 0$:

$$z(\tau) = e^{-\frac{\delta\tau}{2}}\left(\text{ce}_r(q,\tau) + \text{se}_r(q,\tau)\right) \tag{25}$$

$\text{ce}_r(q,\tau)$ and $\text{se}_r(q,\tau)$ are the elliptic cosine and sine functions [27], respectively with $r = a - \delta^2/4$. For $q = 0$ these functions reduces to

$$\text{ce}_r(0,\tau) = \tau\cos\sqrt{a - \frac{\delta^2}{4}}, \tag{26}$$

$$\text{se}_r(0,\tau) = \tau\sin\sqrt{a - \frac{\delta^2}{4}}. \tag{27}$$

[2] Wolfram Research, Inc. See `http://www.wolfram.com`

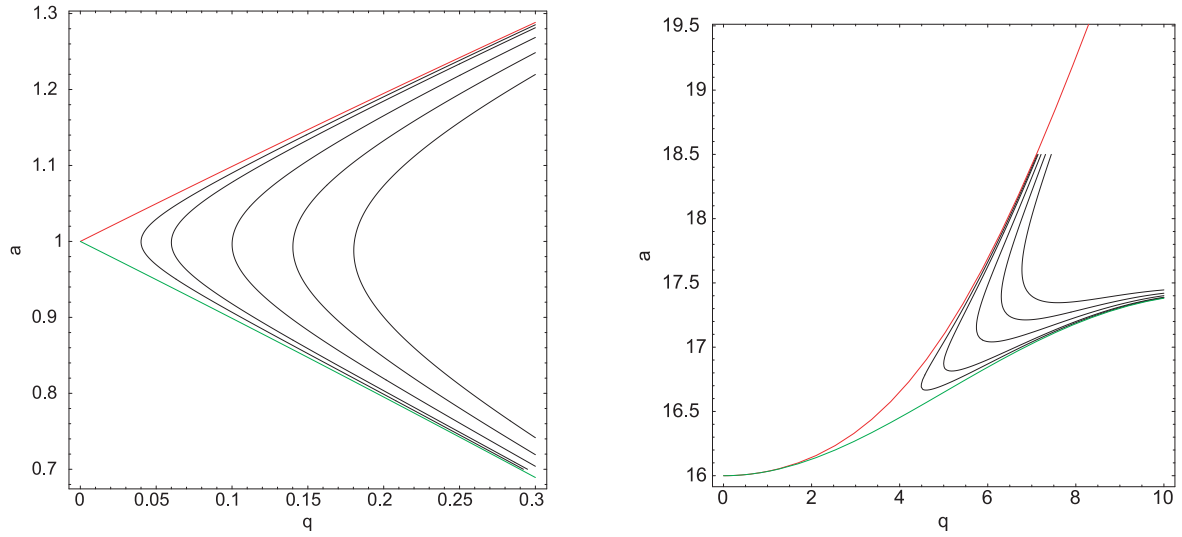

Fig. 10. Boundaries of the unstable areas of the Mathieu equation for different damping constants belonging to the different isocurves. From left to right the constants are $\gamma = 0.02,\ 0.03,\ 0.05,\ 0.07,\ 0.09$. The picture on the left belongs to $a = 1$ $(n = 1)$ and the picture of the right to $a = 16$ $(n = 4)$.

The expression in parenthesis in equation (25) is a periodic function of τ. Thus comparing equation (25) with equation (23) we can set the real part of the floquet exponent equal to the damping constant δ, modulo 2.

In order to obtain μ we have to solve the roots of the Hill's determinantal equation [29]. As shown by Whittaker and Watson the Hill determinant $\Delta(i\mu)$ depending on μ can be written in a compact form:

$$\Delta(i\mu) = \Delta(0) - \frac{\sin^2\left(\frac{1}{2}\pi i\mu\right)}{\sin^2\left(\frac{1}{2}\pi\sqrt{\tilde{a}}\right)} \tag{28}$$

$\Delta(0)$ is the Hill determinant belonging to $\mu = 0$ with the dimension $(2l+1)\times(2l+1)$, $l \in \mathbb{N}$, where $l \to \infty$. For the first three orders $l = 1, 2, 3$ the Hill determinants $\Delta(0) \equiv \Delta_l$ have the following forms:

$$\Delta_1 = 1 + \frac{2q^2}{(4-\tilde{a})\tilde{a}}$$

$$\Delta_2 = \frac{2q^2\left(1 - \frac{q^2}{(4-\tilde{a})(16-\tilde{a})}\right)}{(4-\tilde{a})\tilde{a}} + \left(1 - \frac{q^2}{(4-\tilde{a})(16-\tilde{a})}\right)^2$$

$$\Delta_3 = 2q^2\left(1 - \frac{q^2}{(16-\tilde{a})(36-\tilde{a})}\right) \times \frac{\left(1 - \frac{q^2}{(4-\tilde{a})(16-\tilde{a})} - \frac{q^2}{(16-\tilde{a})(36-\tilde{a})}\right)}{(4-\tilde{a})\tilde{a}} + \left(1 - \frac{q^2}{(4-\tilde{a})(16-\tilde{a})} - \frac{q^2}{(16-\tilde{a})(36-\tilde{a})}\right)^2.$$

We only get a solution when the determinant $\Delta(i\mu)$ vanishes, thus leading to

$$\sin^2\left(\frac{1}{2}\pi i\mu\right) = \Delta(0)\sin^2\left(\frac{1}{2}\pi\sqrt{\tilde{a}}\right) =: f(\tilde{a}, q). \tag{29}$$

This equation can be interpreted as a functional system of isocurves. It means that for a given μ we can determine all a and q values belonging to the same Floquet exponent.

Inserting now the ansatz of equation (24) into the left side of equation (29) we immediately get:

$$\sin\left(i\frac{\pi}{2}(\gamma + i\,n)\right) = i\sinh\left(\frac{\pi}{2}\gamma\right)\cos\left(\frac{\pi}{2}n\right) - \cosh\left(\frac{\pi}{2}\gamma\right)\sin\left(\frac{\pi}{2}n\right). \tag{30}$$

Two cases have now to be distinguished: in case of $n = 2m$ *even* we have

$$\cos\left(\frac{\pi}{2}n\right) = \cos(\pi m) = (-1)^m$$
$$\sin\left(\frac{\pi}{2}n\right) = \sin(\pi m) = 0,$$

leading to

$$\Delta_l \sin^2\left(\frac{\pi}{2}\sqrt{\tilde{a}}\right) = -\sinh^2\left(\frac{\pi}{2}\gamma\right). \tag{31}$$

In case of $n = 2m+1$ *odd* we get

$$\Delta_l \sin^2\left(\frac{\pi}{2}\sqrt{\tilde{a}}\right) = \cosh^2\left(\frac{\pi}{2}\gamma\right). \tag{32}$$

So for a given constant γ we have got an analytic expression for the isocurve $f(a, q)$ for any order l of the Hill determinant. As examples the instability areas starting at $a = 1$ and $a = 16$ are plotted in Figure 10. The outer curves mark the boundaries of the undamped instability regions. When we plot the minimum q-value of the

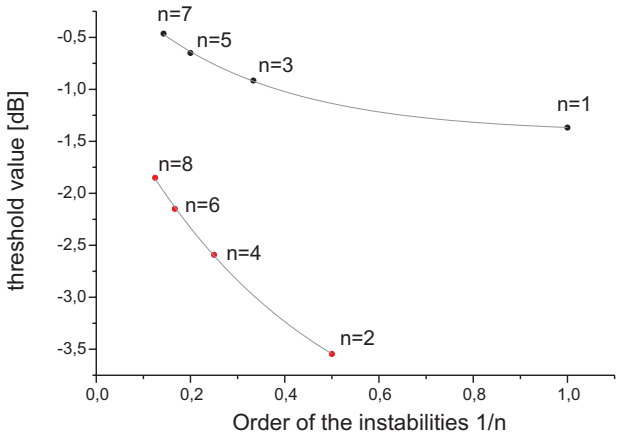

Fig. 11. Graphical plot of the threshold value versus the reciprocal value of the order of the subharmonics for low damping constant. We observe an even-odd staggering for $\gamma = 10^{-4}$. For the simulation Hill determinants with dimension $l = 30$ were solved.

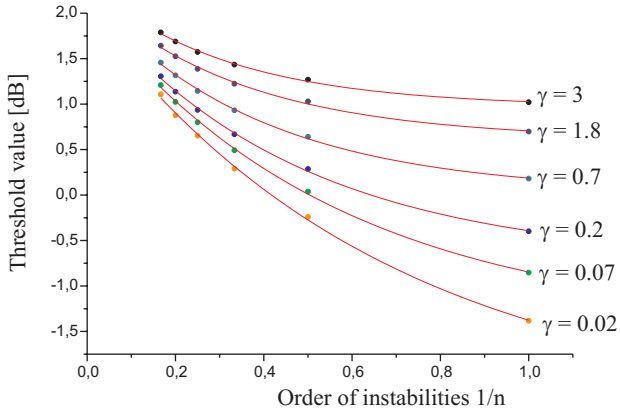

Fig. 12. Threshold excitation for high damping constants. The subharmonics belonging to even and to odd orders lie on one single curve. For the simulation Hill determinants with dimension $l = 30$ were solved.

isocurves belonging to the same damping constant versus the reciprocal value of the order of the instability n, we get for a low damping constant ($\gamma = 10^{-4}$) an even-odd staggering as experimentally observed (Fig. 11). For a high value of γ all orders of the instabilities lie on the same curve (Fig. 12).

4 Summary and conclusions

We have investigated nonlinear dynamical processes of a parametrically excited electron cloud stored in a Penning trap. By driving the axial eigenmotion of the electrons with an external periodical radiofrequency field we observed phenomena which are a characteristic of an excited anharmonic oscillator: the axial resonance of an electron cloud splits into two asymmetric components which can be assigned to the center-of-mass and the to the individual electrons' oscillation. The asymmetry arises in the case of the center-of-mass component from trap imperfections while for the individual component the space charge potential leads to unharmonicities. Furthermore we have observed resonances appearing at frequencies $\omega = 2\omega_z/n$. These resonances show a similar substructure. The appearance of subharmonic resonances require a minimum value of the excitation amplitude in order to overcome damping. The damping mechanism is assumed to arise mainly from induced image charges. For small values of the damping constant the threshold amplitude shows a staggering between even and odd values of the subharmonics while for larger damping constants this behaviour vanishes. This can be understood by solving the corresponding equations of motion and explains different experimental observations.

We demonstrated that a simple system of parametrically excited electrons confined in a Penning trap serves well for a study of nonlinear dynamical processes. The investigation of harmonic and anharmonic systems being exposed to an external periodical perturbation can be used for a variety of applications. A possible application lies in quantum computing. Reducing the electron cloud to a single electron which is parametrically excited can provide the possibility for building a "1-bit-memory" [41].

Furthermore the phenomena of individual and collective motion of an ensemble of charged particles can also be observed in plasma physics [42] in which neutral plasmas acquire for certain densities collective characteristics where physical quantities like the Debye wavelength $\lambda_D = \sqrt{kT/\varepsilon_0 ne^2}$ and the plasma frequency $\omega_p = \sqrt{q^2 n/\varepsilon_0 m}$ play an important role.

Finally subharmonics also occur in solid state physics when studying the interaction of optical waves in photorefractive materials [43]. These photorefractive media can be used in optical signal processing for a wide range of technical application. It is interesting to note that there exist an analogy between the spatial subharmonics observed in photorefractive crystals and the temporal subharmonic instabilities we observed on stored charged particles. From the theoretical point of view the analogy is due to the fact that the Kukhtarev's material equations [44] governing the photorefractive moving gratings can be transformed into a nonlinear spatio-temporal differential equation for space charge fields which is formally equal to the damped Mathieu differential equation.

G.T. gratefully acknowledges M. Kretzschmar for fruitful discussions about the theoretical aspects of the experimental results. Furthermore we thank R.F. Garcìa for the repeated measurements of the threshold values, thus confirming our previous results.

Appendix

The asymmetric peak shape with a tail on the low frequency side observed for the first order individual and center-of-mass resonance (see Figs. 6 and 7) arising from anharmonicities emerging from higher order to the ideal

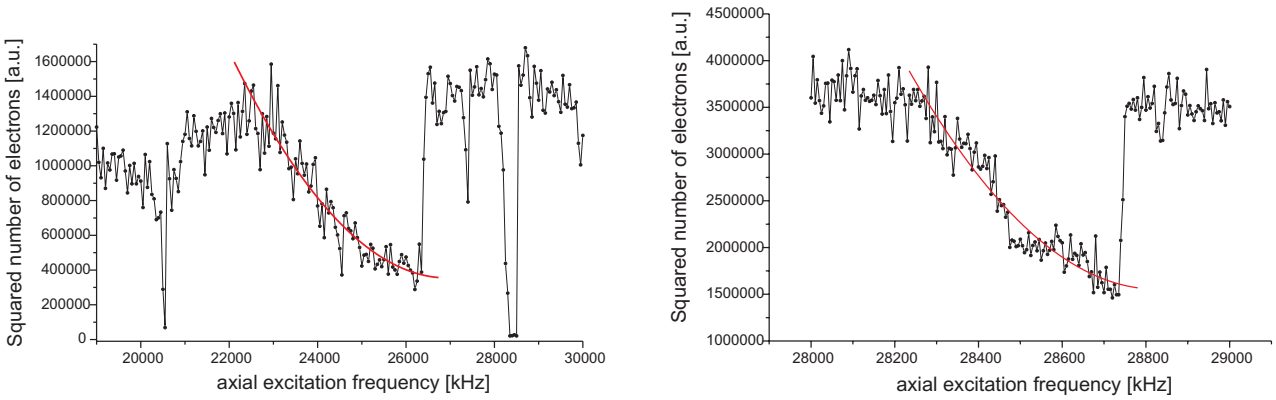

Fig. 13. The individual (left) and the centre-of-mass (right) resonance with squared number of the number of electrons. The fitted curves are given by equation (43).

quadrupole storage potential. This "real" electrostatic potential can be developed in a series of Legendre polynoms:

$$\Phi(|\boldsymbol{r}|) = U_0 \sum_{k=1}^{\infty} C_k \left(\frac{r}{r_0}\right)^k P_k(\cos\theta). \tag{33}$$

For the following theoretical consideration we only consider the octopole and the decapole term characterized by the Legendre coefficients C_4 and C_6, respectively, as the most likely leading terms of the perturbation. For the equation of motion of the electron in axial direction we can generally write:

$$\ddot{z} + \gamma_z \dot{z} + \omega_z^2 z + \lambda_4 \omega_z^2 z^3 + \lambda_6 \omega_z^2 z^5 = k\omega_z^2 \cos\omega_d t \tag{34}$$

which is valid for the individual as well as for the center-of-mass motion. γ_z is the axial damping constant, k is the parametric excitation amplitude and ω_d is the r.f. driving frequency given by:

$$\omega_d = 2(\omega_z + \varepsilon), \tag{35}$$

with $\varepsilon \ll \omega_z$. Furthermore λ_4 and λ_6 are related to the Legendre coefficients in the following way [45]:

$$\lambda_4 = \frac{2C_4}{1+C_2} \quad \text{and} \quad \lambda_6 = \frac{3C_6}{1+C_2} \tag{36}$$

C_2 represents the pure quadrupole term which can be normalized to 1.

Close to the resonance $2(\omega_z + \varepsilon)$ the response function of the excited system increases exponentially, when exceeding a certain critical value of the amplitude k_{thr} which is defined by [9,10]

$$k_{\text{thr}} = \frac{2\gamma_z}{\omega_z}. \tag{37}$$

For a fixed value of the amplitude $k > k_{\text{thr}}$ the parametric excitation is limited to the frequency interval $\varepsilon_- < \varepsilon < \varepsilon_+$, where $\varepsilon_\pm$ have the following form:

$$\varepsilon_\pm = \pm\frac{\omega_z}{4}\sqrt{k^2 - k_{\text{thr}}^2} \tag{38}$$

In order to solve the equation of motion in (34) we can make the following ansatz:

$$z(t) = A(t)\cos\left((\omega_z + \varepsilon)t + \varphi(t)\right). \tag{39}$$

Under the assumption that the amplitude $A(t)$ and the phase $\varphi(t)$ of the system only have a weak dependence on time, we get for the conditions $\varepsilon \ll \omega_z$ and $\gamma_z \ll \omega_z$ two coupled differential equations:

$$\frac{dA}{dt} = -\frac{\gamma_z}{2}A\left\{1 - \frac{k}{k_{\text{thr}}}\sin(2\varphi)\right\} \tag{40}$$

$$\frac{d\varphi}{dt} = -\varepsilon + \frac{1}{4}h\omega_z\cos(2\varphi) + \frac{3}{8}\lambda_4\omega_z A^2 + \frac{5}{16}\lambda_6\omega_z A^4. \tag{41}$$

For the stationary case the following solutions result:

$$\sin(2\varphi) = \frac{k_{\text{thr}}}{k} \tag{42}$$

$$\frac{5\lambda_6\omega_z A^4}{16} + \frac{3\lambda_4\omega_z A^2}{8} + (\varepsilon_+ - \varepsilon) = 0. \tag{43}$$

By fitting now a parabolic function to the lower frequency tail of the $2\omega_z$-resonance we can extract the values for λ_4 and λ_6, thus allowing us to determine the Legendre coefficients C_4 and C_6. From our data (see Fig. 13) we obtain for the individual resonance the values

$$C_4 \approx -9.8 \times 10^{-3}$$
$$C_6 \approx 3.8 \times 10^{-5}$$

whereas for the center-of-mass resonance we get

$$C_4 \approx -7.5 \times 10^{-2}$$
$$C_6 \approx 2.8 \times 10^{-4}.$$

Note that values for the center-of-mass resonance are roughly one order of magnitude bigger than the values for the individual resonance. This might be due to the fact in the case of the stochastic, incoherent motion of the electron cloud the single electrons feel the Coulomb potential of the neighbouring electrons which add to the

anharmonicities of the storage potential. In contrast, the centre-of-mass of the electron cloud does not experience any space charge because of the lacking Coulomb interaction and the anharmonicities are entirely due to the trap imperfections.

References

1. R.S. van Dyck Jr et al., Phys. Rev. Lett. **59**, 26 (1987)
2. G. Werth, Phys. Scripta **T59**, 206 (1995)
3. H. Häffner et al., Phys. Rev. Lett. **85**, 5308 (2000)
4. R.S. van Dyck Jr et al., in: *Atomic Physics at Accelerators*, edited by D. Lunney, G. Audi, H.-J. Kluge (Kluwer Acad. Press, 2001), p. 163
5. S. Rainville et al., in: *Atomic Physics at Accelerators*, edited by D. Lunney, G. Audi, H.-J. Kluge (Kluwer Acad. Press, 2001), p. 215
6. T. Fritjoff et al., in: *Atomic Physics at Accelerators*, edited by D. Lunney, G. Audi, H.-J. Kluge (Kluwer Acad. Press, 2001), p. 231
7. J.J. Bollinger et al., Phys. Rev. A **48**, 525 (1993)
8. References in: *Proc. Non-Neutral Plasma Workshop*, edited by F. Anderegg, L. Schweikhardt, F. Driscoll, AIP Conf. Proc. **606** (2002)
9. J. Tan, G. Gabrielse, Phys. Rev. A **48**, 3105 (1993)
10. C.H. Tseng, G. Gabrielse, Appl. Phys. B **60**, 95 (1995)
11. G. Tommaseo et al., Eur. Phys. J. D **25**, 113 (2003)
12. G. Brown, G. Gabrielse, Rev. Mod. Phys. **58**, 233 (1986)
13. P. Paasche et al., Eur. Phys. J. D **18**, 295 (2002)
14. D.J. Bate et al., J. Mod. Opt. **39**, 305 (1991)
15. M. Kretzschmar, Phys. Scripta **46**, 544 (1992)
16. R. Alheit et al., Phys. Rev. A **56**, 4023 (1997)
17. M. Vedel et al., Appl. Phys. B **66**, 191 (1998)
18. B. Schäfer, Diploma thesis, Inst. f. Phys., Mainz (1999)
19. L.D. Landau, E.M. Lifschitz, *Lehrbuch der theoretischen Physik - Bd. I Mechanik*, Hrsg. von G. Heber (Akademie-Verlag, Berlin, 1969)
20. M. Minkorsky, *Nonlinear Oscillations* (D. Van Nostrand Company, Inc., Princeton, New Jersey, 1962)
21. E. Butikov, Comput. Sci. Engineer. **1**, 76 (1999)
22. L. Mandelstam, N. Papalexi, Z. Phys. **73**, 223 (1932)
23. L. Mandelstam et al., J. Tech. Phys. (U.S.S.R.) **2**, 81 (1934)
24. H. Poincaré, *Méthodes nouvelles de la mécanique céleste* (Gauthier-Villars, Paris, 1892), tome 1, p. 79
25. A.M. Ljapunow, *Das allgemeine Problem der Stabilität einer Bewegung* (Onti, 1935)
26. N.W. McLachlan, *Theory and Applications of Mathieu Functions* (Oxford University Press, New York, 1947)
27. J. Meixner, F.W. Schäfke, *Mathieusche Funktionen und Sphäroidfunktionen* (Springer-Verlag, Berlin, 1954)
28. M.J.O. Strutt, Math. Ann. **99**, 625 (1928)
29. E.T. Whittaker, G.N. Watson, *A Course of Modern Analysis* (Cambridge at the University Press, 1958), chapter XIX
30. G. Kotowski, Z. Angew. Math. Mech. **23**, 213 (1943)
31. R.D. Knight, Int. J. Mass Spectrom. Ion Phys. **51**, 127 (1983)
32. N.N. Bogoljubow, J.A. Mitropolski, *Asymptotische Methoden in der Theorie der nichtlinearen Schwingungen* (Akademie-Verlag, Berlin, 1965)
33. G. Rettinghaus, Ph.D. thesis, Bonn University (1965), unpublished
34. D. Wineland, H.G. Dehmelt, Int. J. Mass Spectrom. Ion Phys. **16**, 338 (1975)
35. M.A.N. Razvi et al., Phys. Rev. A **58**, R34 (1998)
36. B.A. Collings, D.J. Douglas, J. Am. Soc. Mass Spectrom. **11**, 1016 (2000)
37. R.S. van Dyck Jr et al., Phys. Rev. A **40**, 6308 (1989)
38. J.V. Porto, Phys. Rev. A **64**, 023403 (2001)
39. D.J. Wineland, H.G. Dehmelt, J. Appl. Phys. **46**, 919 (1975)
40. P. Hagedorn, Z. Angew. Math. Mech. **48**, T256 (1968)
41. C.H. Tseng et al., Phys. Rev. A **59**, 2094 (1999)
42. J.P. Schermann, F.G. Major, Appl. Phys. **16**, 225 (1978)
43. C.H. Kwak, E.-H. Lee, Electr. Telecomm. Res. Inst. J. **16**, 13 (1995)
44. N.V. Kukhtarev, Ferroelectrics **22**, 949 (1979)
45. G. Gabrielse, Phys. Rev. A **29**, 462 (1984)